NUMERICAL AND EXPERIMENTAL ANALYSIS OF CONCRETE BLOCK PRISMS UNDER COMPRESSION

A. A. FREITAS

PhD Student
University of S.Paulo, S.Paulo, Brazil

M. A. RAMALHO

M. R. S. CORRÊA

Associated Professor
University of S.Paulo, S.Paulo, Brazil

A. TALIERCIO

Full Professor
Politecnico di Milano, Milan, Italy

SUMMARY

This paper presents a comparison between experimental and numerical analysis of concrete block prisms under compression loads. The main goal of the study is to simulate the behavior of prisms based on the behavior of blocks and mortar joints using a numerical non-local damage model specially developed for quasi-brittle materials. An experimental program, with displacement control, is carried out to determine damage parameters and the complete load-displacement diagram of the prisms. Numerical models are then used to evaluate the behavior of the prisms. Obtained results show that the considered non-local damage model is able to predict the failure and the softening regime of the prisms.

INTRODUCTION

Damage numerical models can be pivotal to evaluating the non-linear behavior of some structural elements. When assessing brittle materials, damage-based procedures may be indispensable to simulate the medium loss of rigidity due to micro-cracks formation, which can lead it to failure. Kachanov 1958 was perhaps the first to have mentioned the damage concept as it is currently known. Another important contribution can be ascribed to Rabotnov 1969, who proposed a damage variable that could be used to reduce initial rigidity and the strength of the material. Recently, after the formalization of the so-called Continuum Damage Mechanics (Lemaitre and Chaboche 1985), the development of this research field was quick and varied. It is noteworthy that for this study the damage mechanics applied to brittle materials is especially important, for instance structural masonry.

About the importance of the study presented here, it is worth highlighting that many codes adopt the structural masonry strength based on prism strength. Therefore, the numerical evaluation of the prism behavior based on its components behavior, units and mortar, is a very interesting way to obtain important information about the masonry behavior itself. Obviously, if this knowledge is obtained based on experimental results only for the masonry components this procedure will save a significant amount of time and money.

EXPERIMENTAL PROGRAM

The experimental program was accomplished at the Department of Structural Engineering of University of São Paulo (USP). The tests were carried out both on masonry components, blocks and mortar specimens, and on two-block prisms built with the same components.

The hollow concrete blocks had a nominal strength of 4.5 MPa and the dimensions were 140, 190 and 390 mm (width, height and length), Figure 1a. The cylindrical mortar specimens dimensions were 50 and 100 mm (radius and height), Figure 1b. Two mortar mix proportions, in volume, were considered: 1:0.5:4.5 (Type ii of BS 5628 1992) and 1:1:6 (Type iii of BS 5628 1992).

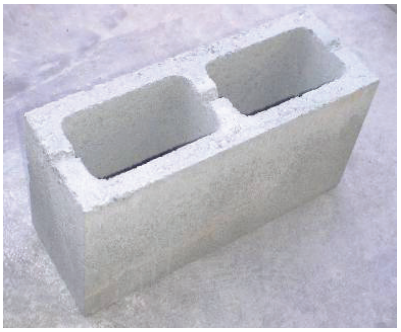

(a) Concrete blocks

(b) Mortar specimens

Figure 1. Concrete blocks and mortar specimens

All the axial compression tests for components and prisms were performed in order to obtain the complete force-displacement curve for the specimens, in other words, the behavior of the specimens from the initial loading stage until the complete failure of the material. Therefore, a hydraulic servo-controlled press under displacement control at 1 μm/s was used. Despite the fact the press had an internal displacement control, four additional devices for displacement measurement (LVDT) were also used in all the performed tests, see Figure 2.

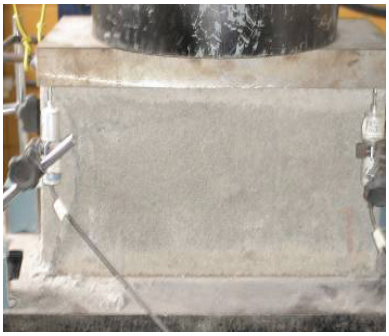

(a) Block

(b) Mortar specimen

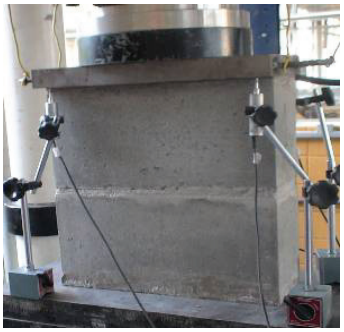

(c) Prism

Figure 2. Axial compression tests

In order to characterize the units, eight concrete blocks were tested. From the obtained load-displacement diagrams it was possible to define a representative behavior for the units. Figure 3 demonstrates all of the obtained results for the prisms and the adopted block diagram that will be used for all the numerical prism models, as can be observed in details in a following section.

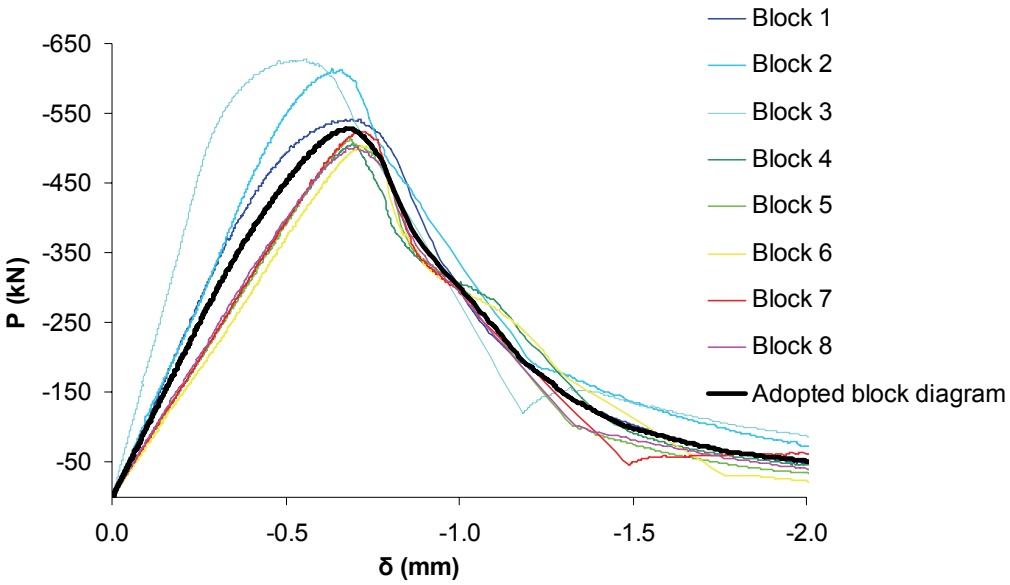

Figure 3. Load-displacement diagrams for the units.

Six prisms were tested under axial compression. Three of them were built using the BS 5628 type ii mortar and the other one with the type iii mortar. For all of the prisms the mortar bed joint was 10 mm thick. The complete load-displacement diagrams were obtained for all the prisms in order to facilitate comparing them to those obtained numerically. The obtained diagrams are presented in a following section, where the numerical results are compared to the experimental ones.

It is worth noting that for each tested prism a mortar specimen was taken to be considered representative of the prism mortar joint. Each one of those mortar specimens was also tested in order to obtain the complete load-displacement diagram. Those diagrams will be used to obtain the damage parameters for the mortar, which can be seen in detail in a following section. In fact, the cylindrical mortar specimen prepared in a steel mould does not capture the in-situ properties of the mortar bed joint. However, this type of specimen was adopted because it is a standard test and one of the aims of the present research project was the validation of the proposed procedure considering only standard tests for the masonry components.

DAMAGE MODEL

The numerical analysis performed in the present paper is based on a damage model procedure originally developed by Papa and Taliercio 2005. This model was adapted by Ramalho et. al. 2005 and implemented in the FEAP® program (FEAP 2002). The obtained local damage procedure is reliable and efficient for evaluating the stress-strain behavior from the initial

loading stage until the peak load of the structural element, especially when it is submitted to loadings in which the compression is the main effect, Anzani et. al. 2005.

However, the numerical local damage procedure, considering brittle materials under a not constant strain field and using finite elements analysis, usually leads to a strong strain concentration. It means to obtain spurious results and strong mesh sensitivity (Jirásek 1998). Typically, the inelastic strains are concentrated in an element or in narrow bands of elements, whereas the major part of the structure is nearly unstrained. As a consequence, it is impossible to evaluate the complete load-displacement diagram, especially for the softening region, i.e. from the peak load to the complete failure of the material.

Considering these numerical problems, the damage procedure was changed and a non-local damage model based on a strain averaging procedure was implemented. In this case the strains at each point are calculated by means of a weighted averaging over a spatial neighborhood of the point (Ramalho et al. 2007).

Obviously, it is not the main goal of this paper to discuss in detail the damage model used in the numerical analysis. However, some of the model's features are explained in order to show the main parameters that should be considered. Hence, it is important to mention that the damage phenomena are macroscopically taken into account through a symmetric, second-order tensor D. In finite form, the nonlinear stress-strain law of the material reads:

$$\varepsilon = C(D)\,\sigma \tag{1}$$

where C(D) is the fourth-order flexibility matrix of the damaged material that depends on the damage tensor D.

The eigenvalues and the normalized eigenvectors of the damage tensor will be denoted by D_α and n_α (α = I, II, III), respectively. Any one of the planes of damage-induced orthotropy is somehow associated to a plane micro-crack that forms in the solid. Once any damage direction is activated, its orientation is supposed to remain fixed throughout the rest of the stress history.

The damage process driving variable is supposed to be an equivalent strain measure, $y = \frac{1}{2}\,\varepsilon^2$. As the maximum eigenvalue of y attains a critical value; y_{0T} or y_{0C}, according to the sign of the associated strain; the first damage direction (n_I) is activated. An additional damage direction, n_{II}, can be activated in the plane orthogonal to n_I if the maximum direct component of y, that is, $y_{hh} = n_h \cdot (y \cdot n_h)$, with $n^h \perp n_I$, attains the damage threshold. The third possible damage direction is necessarily $n_{III} = n_I \wedge n_{II}$.

Neglecting creep-induced damage, each principal value of the damage tensor is supposed to evolve according to the law:

$$D_\alpha = 1 - \frac{C_H}{1 + A_H \left\langle y_{hh} - y_{0H} \right\rangle^{B_H}},\ \alpha = I, II, III. \tag{2}$$

Here, $\langle * \rangle$ are McAuley brackets and A_H, B_H and C_H are material parameters, which take different values according to the sign of the strain component that activates damage (H=T for tension; H=C for compression).

It is worth mentioning that in the initial stages of the loading, before any damage direction is activated, the material can be considered as elastic-linear and in this case the Young's modulus and the Poisson coefficient are also necessary.

Besides the local damage parameters, it is also pertinent defining the spatial neighborhood of the point so that is possible to consider the non-local damage procedure. This spatial region is usually a sphere, characterized by its radius. In this paper its radius is adopted as the smallest value for which the numeral procedure does not present strain concentration, i.e. mesh dependency effects.

Basically there are two procedures to verify the event of strain concentration in the analysis. First, the load-displacement diagram presents a clear discontinuity just after the peak load. Second, the number of iterations increases suddenly for the load step just after the load peak and sometimes it is not even possible to reach the convergence value. On the other hand, if the strain concentration phenomenon is not present, then the load-displacement diagram does not present any discontinuity and there is not a significant difference between the number of iterations for the several load steps of the analysis.

DAMAGE PARAMETERS

Initially, finite element meshes were assembled for the concrete block and the mortar specimens, Figure 4. Displacements were restrained according X, Y and Z axes, both at the top and at the bottom of the meshes, while the displacements that simulated the test loading scheme were applied parallel to the Z axis at the top of the model. Four-noded tetrahedra finite elements were adopted for the mortar specimens meshes while eight-noded hexahedra finite elements were used for the block mesh. The number of elements was 663 and 1608, respectively, for the mortar specimens and for the block.

The Young's modulus (E) and Poisson coefficient (ν) were adopted taking only into account the obtained values of the experimental program for each component. However, the damage parameters A_c, B_c and C_c, see Equation 2, were evaluated so that the numerical diagram of a component, block or mortar specimen, would be as similar as possible to the experimental load-displacement diagram obtained for the same component. Note that for the block the adopted block diagram, shown in Figure 3, was considered, while the six mortar specimens had their own diagram to be considered.

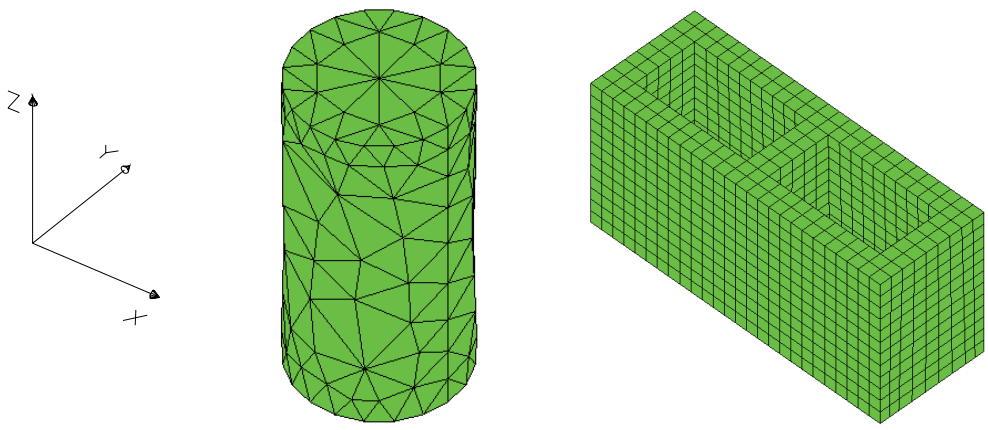

(a) Mortar specimen (b) Block

Figure 4. Finite element meshes.

After assessing the local damage parameters it was possible to evaluate the spatial neighborhood radius (r_{nl}) for considering non-local damage. As previously described, in this paper this radius was considered as the smallest value for which the numeral procedure does not present strain concentration.

Table 1 presents the obtained parameter values for the block and the mortars used to build the prisms. It is relevant to mention that the mortars M1, M2 and M3 could be classified as type ii and the mortars M4, M5 and M5 were type iii (BS 5628 1992). Additionally, it is also important to highlight that the mortar specimen "Mi" was representative of the bed joint of the prism "i".

Table 1. Damage parameters for components.

Parameter	Block	Mortar					
		M1	M2	M3	M4	M5	M6
E (N/mm^2)	6574.80	5078.30	4287.00	4082.20	3840.70	2726.10	4138.80
A_c	1.10×10^6	900	440	755	460	515	330
B_c	2.80	1.10	0.90	1.00	0.90	0.90	0.90
C_c	0.97	1.00	1.00	1.30	1.09	1.09	1.00
r_{nl} (mm)	150	30					
ν	0,20						

In order to exemplify the appearance of the experimental and numerical diagrams, Figure 5 illustrates the obtained results for the block and Figure 6 presents the results for the mortars. The numerical diagrams were obtained using the parameters shown in Table 1 and they will be used to model the prisms presented in the following section.

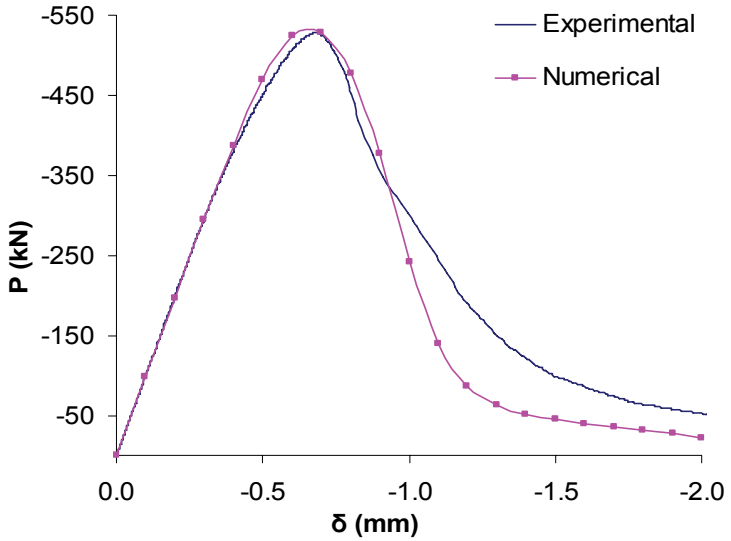

Figure 5. Load-displacement diagram for the block.

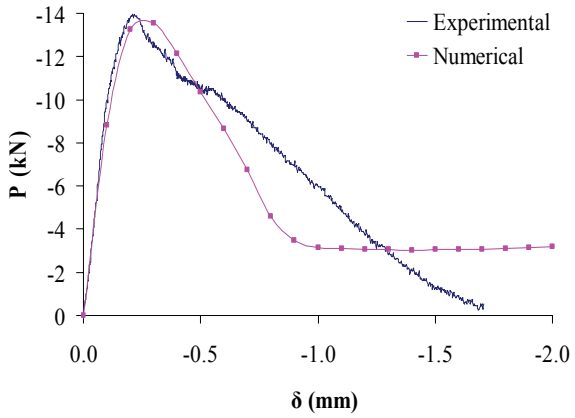

(a) Mortar M1

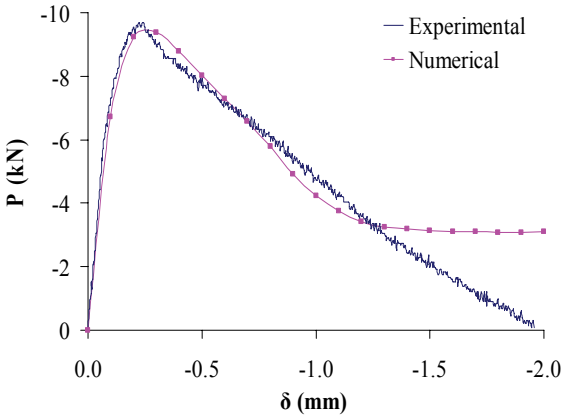

(a) Mortar M2

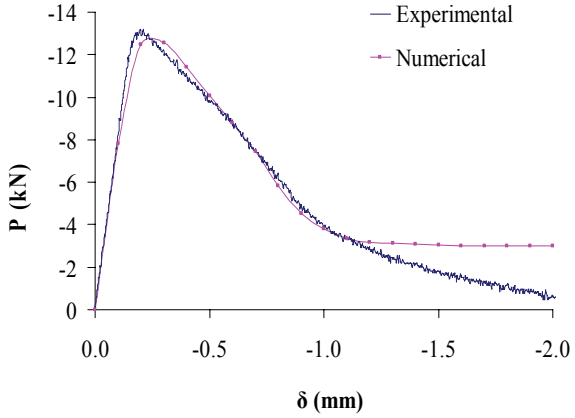

(a) Mortar M3

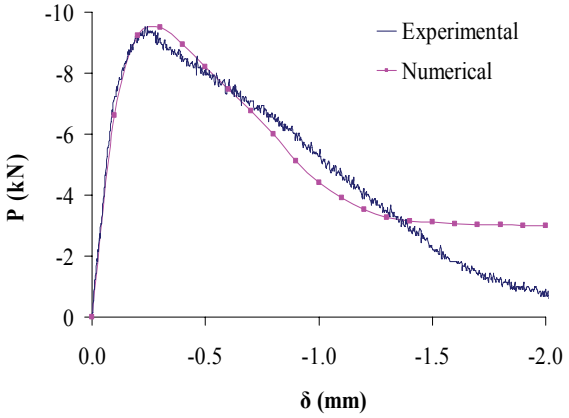

(a) Mortar M4

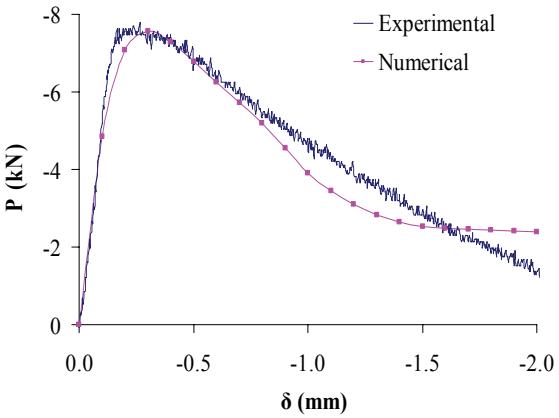

(a) Mortar M5

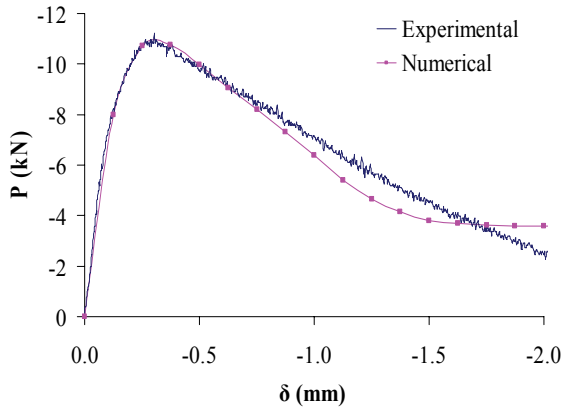

(a) Mortar M6

Figure 6. Load-displacement diagrams for the mortars.

OBTAINED RESULTS FOR THE PRISMS

The assembled mesh for the prisms had 3484 eight-noded hexahedra finite elements and is shown in Figure 7. The parameters shown in Table 1 for the block and the respective mortar were used to model each prism. Similarly to the mortar specimen and the block models, displacements were restrained according X, Y and Z axes, both at the top and at the bottom of the meshes, while the displacements that simulated the test loading scheme were applied according to the Z axis at the top of the model.

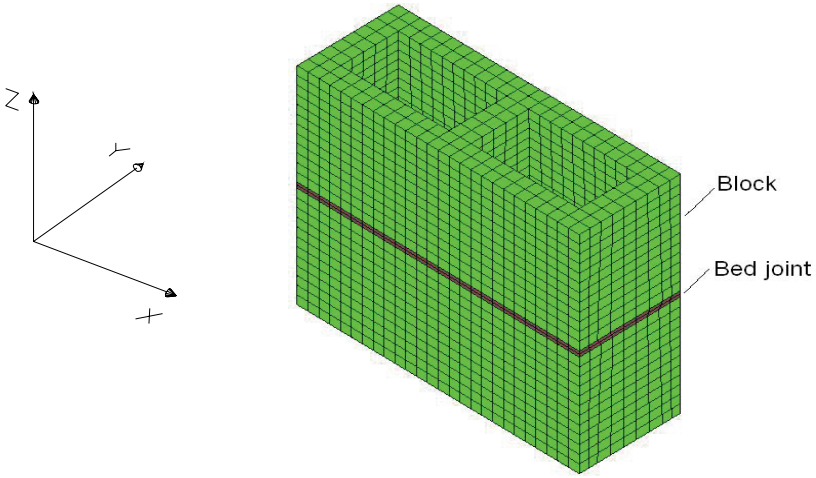

Figure 7. Finite element mesh for the prisms.

Table 2 shows the maximum loads obtained through the numerical model and the experimental program for all the prisms. In this table it is possible to see that the numerical and experimental values are in fact quite close for all cases, presenting a maximum difference of 16.3% between the foreseen numerical value and the measured experimental value. For prism P6 the values were almost identical, with the experimental value only 3.8 % smaller than the numerical foreseen.

Table 2. Maximum load for prisms (kN).

	Prism					
	P1	P2	P3	P4	P5	P6
Experimental	499,75	442,17	371,13	429,43	390,20	405,00
Numerical	434,66	369,71	427,21	375,00	339,00	420,46
Difference (%)	13,0	16,3	15,1	12,6	13,1	3,8

Another significant point to be highlighted is the aspect of the obtained load-displacement diagram from the initial loading stages until the complete failure of the prisms. Figure 8 shows the mentioned diagrams obtained by means of experimental program and numerical model for the six tested prisms. It is possible to deduce that the aspect of the numerical and experimental diagrams is similar for all the prisms. For some of them, for instance prisms P1, P3 and P4 even the displacement associated to the maximum load is accurately foreseen by the numerical model.

Finally, it is interesting to mention that taking into account only the diagrams obtained by numerical procedure; it is possible to note that they are completely coincident considering the elastic-linear stage, in spite of the different Young's modulus for the mortars, Figure 9. Thus, one can conclude that this parameter does not affect significantly the obtained results, probably due to the small thickness of the bed joint relating to the block height. However, this is not the behavior after the damage activation, as also seen in Figure 9.

CONCLUSIONS

The main conclusion is that considering only the parameters obtained by means of the experimental program for its components, i.e. blocks and mortar specimens, it was possible to evaluate numerically the behavior of the prisms under compression with good accuracy.

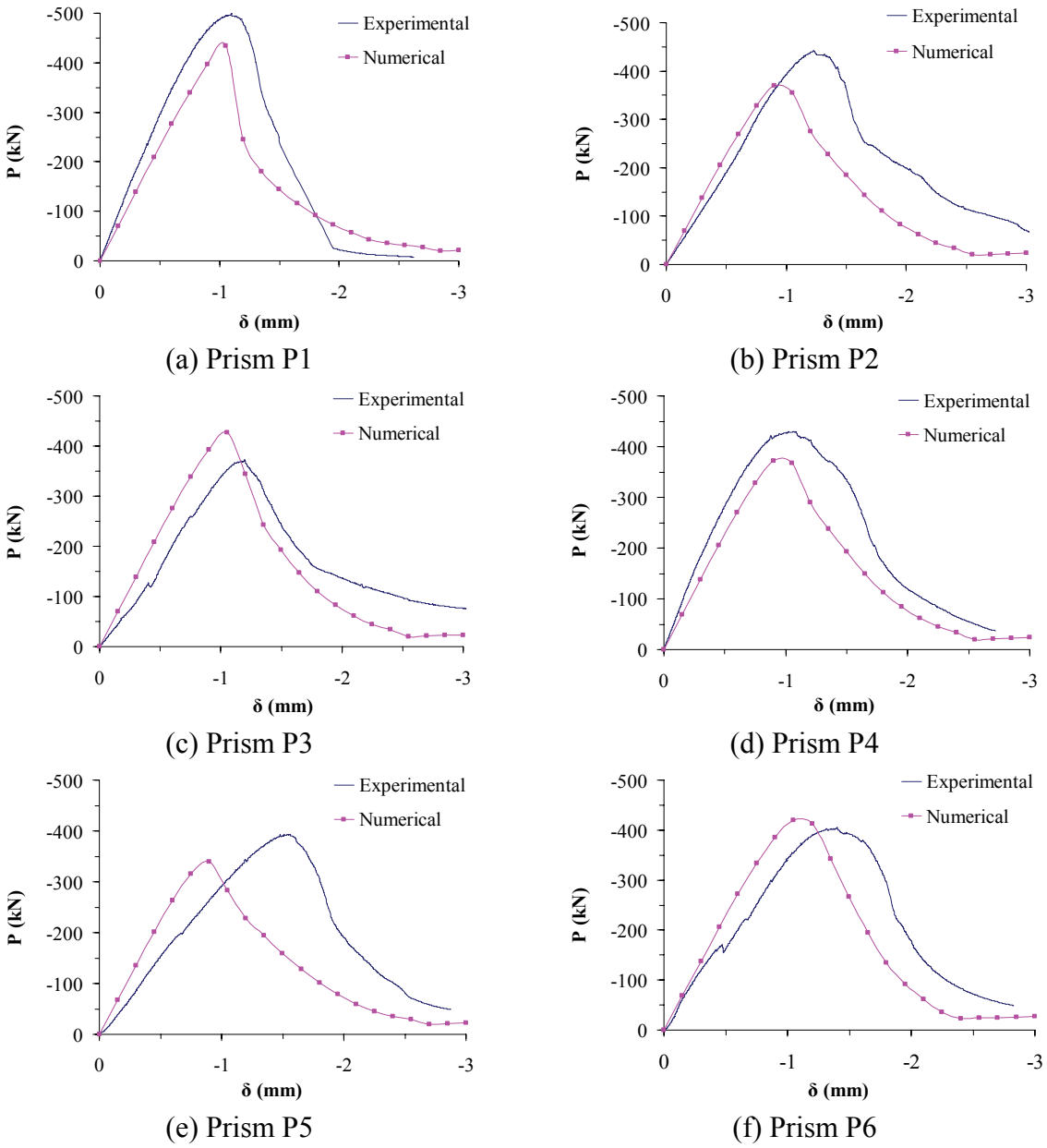

(a) Prism P1 (b) Prism P2

(c) Prism P3 (d) Prism P4

(e) Prism P5 (f) Prism P6

Figura 8. Numerical and experimental load-displacement diagrams for the prisms.

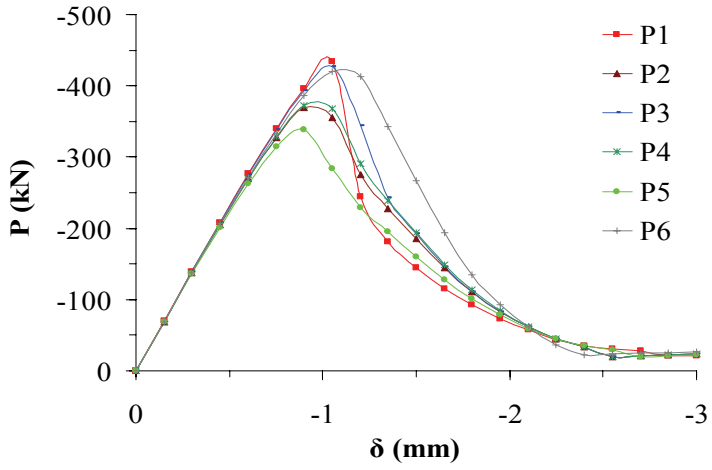

Figure 9. Numerical load-displacement diagrams for the prisms.

Actually, the used non-local numerical model is able to predict different stages of the load-displacement diagram, from its elastic-linear stage until the complete failure of the material. Especially the maximum compression load and its displacement can be evaluated with reasonable precision, demonstrating that the proposed numerical procedure is efficient and reliable to model structural masonry under compression.

Based on the obtained results, it seems clear that the described numerical procedure can be used to evaluate the strength of the structural masonry provided the behavior of the block and the mortar are known in advance.

ACKNOWLEDGMENTS

The authors gratefully acknowledge the support of FAPESP - São Paulo State Research Support Foundation and CNPq – National Council for Scientific and Technological Development.

REFERENCES

Anzani A.; Binda, L.; Ramalho, M. A.; Taliercio, A., "Historic multi-leaf Masonry walls: experimental and numerical research", *Masonry International*, Vol. 18, No. 3, 2005, pp. 101-114.

BS 5628 "Code of practice for structural use of masonry – Part1: Structural use of reinforced masonry", *British StandardIinstitution*, London, 1992.

Jirásek, M., "Nonlocal models for damage and fracture: comparison of approaches", *International Journal of Solids and Structures*, Vol. 35, 1998, pp. 4133–4145.

Kachanov, L. M., "Time of the rupture process of non-linear solid mechanics", *Otd. Tech. Nauk*, Vol. 8, 1958, pp. 28-31.

Lemaitre, J.; Chaboche, J.L., "Mechanics of solid materials", *Cambridge University Press*, 1985.

Papa, E; Taliercio, A., "A damage model for brittle materials under non-proportional monotonic and sustained stresses", *International Journal for Numerical and Analytical Methods in Geomechanics*, Vol. 29, No. 3, 2005, pp. 287-310.

Rabotnov, Y. N., "Creep problems in structural members", *Amsterdam North-Holland*, 1969.

Ramalho, M.A.; Papa, E.; Taliercio, A.; Binda, L., "A Numerical Model for Multi-Leaf Stone Masonry", *International Conference of Fracture, 11*, 2005.

Ramalho, M.A.; Taliercio, A.; Anzani, A.; Binda, L. A; Papa, E., "A Numerical Model for the Description of the Nonlinear Behaviour of Multi-Leaf Masonry Walls", *Advances in Engineering Software*, v.online, #56, 2007.